

Heat Exchange Enhancement by Extremum Seeking Boundary Feedback Control in 3D Magnetohydrodynamic Channel Flow

Lixiang Luo and Eugenio Schuster

Abstract—Electrically conducting fluids are generally favored as heat transfer media for their excellent heat conduction and high boiling point. However, the movement of such fluids under the presence of imposed transverse magnetic fields can generate substantial magnetohydrodynamics (MHD) effects including the need of higher pressure gradients to drive the fluids and lower heat transfer rates due to the laminarization of the flows. In this work we propose an active boundary control to overcome some of these unfavorable MHD effects inside a 3D MHD channel flow. Extremum seeking is used to adaptively tune a fixed-structure boundary controller to maximize in real time a cost function related to heat transfer. The closed-loop controller achieves the ultimate goal of increasing overall heat transfer rate through the channel walls, and therefore enhances the efficiency of the heat exchanger. The velocity dynamics is predicted by a pseudo-spectral solver while the temperature dynamics is predicted by a finite difference solver. Simulation results show the efficiency of the proposed controller.

I. INTRODUCTION

Liquid metals are often considered as the heat transfer media in many cooling systems. Due to their excellent physical properties (high thermal conductivity and high boiling point), they are often considered for extreme conditions, such as those characterizing cooling blankets in magnetic fusion reactors, where high temperatures and strong magnetic fields are present. The main function of the coolant is in this case the absorption of energy from the neutron flux generated by the fusion reactions and the transfer of heat to an external energy conversion system. In addition, if a breeder liquid metal such as liquid-lithium is considered, the blanket can also carry out the breeding of tritium, which is part of the fuel used by the reactor. However, the interaction between the electrically conducting fluids and the magnetic fields used to confine the fuel inside the reactor generates significant MHD effects, which often result in the need of higher pressure gradients to pump the fluid and lower heat transfer rates due to the laminarization of the flow. These MHD effects prevent present liquid-metal cooling systems from producing the heat transfer improvements which might be expected based on the much higher thermal conductivity and boiling point of the coolant. A good review of the present state of research in this area can be found in [1].

Boundary control of fluid systems, implemented through micro electro-mechanical or electro-magnetic actuators and sensors, can be used to counteract the unfavorable MHD

effects. By introducing unsteadiness, boundary controllers have the potential of enhancing mixing and consequently the convection-driven heat exchange rate. Flow control has attracted much interest and dramatically advanced in recent years [2], [3], [4], [5]. In particular, boundary control of MHD flows has been considered for many years [6], [7], [8], [9], [10]. Research subjects range from strongly coupled MHD problems, like liquid metal and melted salt flows, to weakly coupled MHD problems, like salt water flows. Nevertheless, early research mostly focused on passive and open loop control, partly due to the complexity of the coupled MHD equations. Unfortunately the nonlinearities and uncertainties of the system usually limit the effectiveness of these open-loop controllers, which are not optimized with respect to the varying flow conditions. The addition of heat transfer analysis further adds to the complexity and the work carried out on direct enhancement of heat transfer is limited.

Our prior work includes the development of a feedback control scheme for mixing enhancement in a 2D MHD flow [11]. The effectiveness of the proposed controller in enhancing heat transfer was illustrated in [12], where a simple traveling-wave-like boundary controller was also investigated for comparison. Numerical simulations confirmed that the closed-loop control scheme is more effective than the simple open-loop control law. However, subsequent research revealed that adaptive tuning of some parameters of the open-loop controller could result in an much improved performance in 2D MHD channels [13]. In this work we extend this approach to 3D MHD channel flows, which pose a completely new set of challenges.

The geometric setting is given in Fig. 1, with a cross-section shown in Fig. 2. The channel is considered periodic in both x and z directions and bounded in the y direction by the bottom and top walls. An electrically conducting fluid with constant inlet temperature T_i flows under the presence of an imposed transverse magnetic field B_0 through a section of a 3D channel with high-temperature walls (T_p and T_b), and eventually leaves this section with higher outlet temperature T_e after absorbing internal energy from the walls. This setting can be seen as the idealization of a heat exchanger within an electromagnetic environment where an electrically conducting fluid such as a liquid metal is pumped through pipes with the goal of removing heat from the surrounding cooling blanket.

To serve the goal of increasing the energy carried downstream by the fluid, we employ extremum seeking [14] to optimally tune a traveling-wave-like boundary controller, maximizing a cost function related to a heat transfer measure

This work is supported by the NSF CAREER award program (ECCS-0645086). Lixiang Luo (lixiang.luo@lehigh.edu) and Eugenio Schuster (schuster@lehigh.edu) are with the Department of Mechanical Engineering and Mechanics, Lehigh University, Bethlehem, PA 18015, USA.

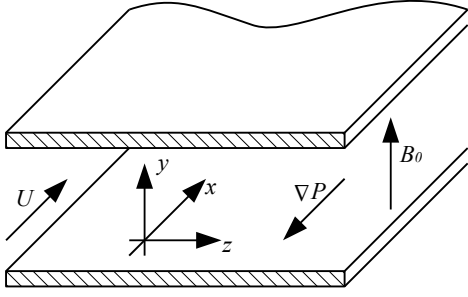


Fig. 1. 3D MHD flow between plates.

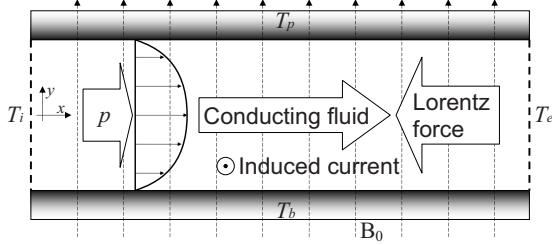


Fig. 2. 3D MHD flow cross section with temperature boundary conditions.

of the MHD channel flow. Extremum seeking is a very effective approach to build real-time feedback controllers based on fixed-structure control laws with tunable parameters [15], [16], [17]. Due to its non-model-based nature, extremum seeking is well suited to overcome the limitations in our MHD problem in terms of uncertainty handling and is capable of capturing the input-output information of the otherwise highly complicated relationship between the control parameters and the heat exchange rate. Furthermore, extremum seeking is very effective in adapting to changing flow conditions in real time. For instance, simulation results show that extremum seeking can quickly retune the feedback controller to a new optimal state after the external magnetic field strength is changed.

This article is organized as follows. In Section 2, we state the simplified MHD equations for incompressible MHD flows and present the associated heat exchange problem. In Section 3, the feedback control scheme is discussed, including a brief introduction to extremum seeking. In Section 4, simulation results are presented for the proposed control scheme in several typical MHD channel flow settings. The complex relationship between the cost function and the to-be-optimized parameters is addressed. Section 5 closes the paper stating conclusions and identifying future work.

II. PROBLEM STATEMENT

We consider a 3D, incompressible, electrically conducting fluid flowing bounded by two parallel plates ($0 < x < L_x = 2\pi$, $0 < z < L_z = \pi$ and $0 < y < 1$), as illustrated in Fig. 1, where an external magnetic field B_0 is imposed perpendicularly to the plates, i.e., in the wall-normal y direction. This is a typical Hartmann flow and its behavior has been well studied over the years [18]. The mass flux Q is fixed. A uniform pressure gradient P_x in the x -direction is required to balance the boundary drag force and the body force due to the

MHD effects. Space variables x, y, z , time t , velocity \mathbf{v} and magnetic induction \mathbf{B} are converted to their dimensionless forms: $x = \frac{x^*}{L}$, $y = \frac{y^*}{L}$, $z = \frac{z^*}{L}$, $\mathbf{B} = \frac{\mathbf{B}^*}{B_0}$, $\mathbf{v} = \frac{\mathbf{v}^*}{U_0}$, $j = \frac{j^*}{U_0 B_0}$, $t = \frac{t^* U_0}{L}$, where L, U_0 and B_0 are dimensional reference length, velocity and magnetic field. Variables denoted by the star notation are dimensional quantities. The vector variables are defined as $\mathbf{v} = u\hat{\mathbf{x}} + v\hat{\mathbf{y}} + w\hat{\mathbf{z}}$, $\mathbf{B} = B^u\hat{\mathbf{x}} + B^v\hat{\mathbf{y}} + B^w\hat{\mathbf{z}}$, where $\hat{\mathbf{x}}, \hat{\mathbf{y}}$ and $\hat{\mathbf{z}}$ are unit vectors in the x, y and z directions.

In this paper, we consider MHD flows at low magnetic Reynolds numbers ($\text{Re}_m \ll 1$), which are also called simplified MHD (SMHD) flows. In these flows the induced magnetic field is negligible in comparison with the imposed magnetic field. The 3D SMHD channel flow is described by modified incompressible Navier-Stokes (N-S) equations and a Poisson's equation for the electric potential:

$$\begin{aligned} \frac{\partial \mathbf{v}}{\partial t} + (\mathbf{v} \cdot \nabla) \mathbf{v} &= -\nabla p + \frac{1}{\text{Re}} \nabla^2 \mathbf{v} + \text{N} [(-\nabla \phi + \mathbf{v} \times \mathbf{B}_0) \times \mathbf{B}_0], \\ \nabla^2 \phi &= \nabla \cdot (\mathbf{v} \times \mathbf{B}_0) = \mathbf{B}_0 \cdot \boldsymbol{\omega}, \\ \nabla \cdot \mathbf{v} &= 0, \end{aligned} \quad (1)$$

where $\boldsymbol{\omega} = \nabla \times \mathbf{v}$ is the vorticity, $\mathbf{B}_0 = \hat{\mathbf{y}}$ is the imposed magnetic field, which is simply a unit vector due to the non-dimensionalization. A detailed derivation of this model can be found in [18]. Numerical simulations also confirm that under such physical settings, full MHD and SMHD give near identical results, while the former method has to use much smaller time steps (characterized by $\text{CFL} \ll 1$ [19]) than the latter method to ensure convergence [20]. Meanwhile, the dynamics of the temperature field is described by the heat transfer equation:

$$\frac{\partial T}{\partial t} = \frac{1}{\text{Pe}} \nabla^2 T + (\mathbf{v} \cdot \nabla) T. \quad (2)$$

The characteristic numbers appearing in the system equations, including Reynolds number Re , magnetic Reynolds number Re_m , Stuart number N and Péclet number Pe , are defined as $\text{Re} = \frac{U_0 L}{\nu}$, $\text{Re}_m = \mu \sigma U_0 L$, $\text{N} = \frac{\sigma L B_0^2}{\rho U_0}$, $\text{Pe} = \frac{\rho c_p U_0 L}{\lambda}$. The physical properties of the fluid, including the mass density ρ , the dynamic viscosity ν , the electrical conductivity σ , the magnetic permeability μ , the specific heat c_p , and the thermal conductivity λ , are all assumed constant.

The bottom and top walls are assumed non-slip. Hence, the velocity boundary conditions for the SMHD system are given by

$$\frac{\partial \phi}{\partial y} = 0, \quad U = W = 0, \quad V = V_{ctrl} \quad \text{at } y = 0 \text{ and } y = 1,$$

where V_{ctrl} is determined by the proposed boundary control laws. In the uncontrolled cases, $V_{ctrl} = 0$. We assume periodic boundary conditions in the streamwise direction. Temperature boundary conditions of either Dirichlet or Neumann type are specified on all four boundaries, as depicted in Fig. 2. In this work we consider a heat transfer process where the heat is removed from the system through the walls of the channel by a running fluid. The boundary conditions are given as

$$T_i = T_0, \quad T_b = T_p = T_0 + T_d, \quad \frac{\partial T_e}{\partial x} = 0.$$

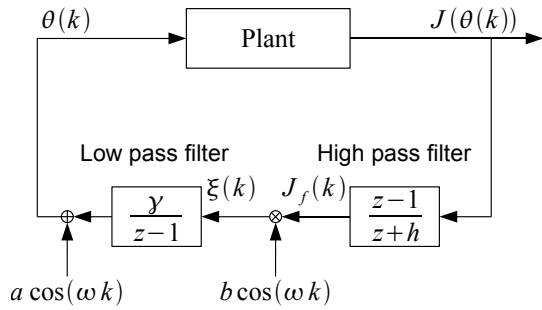


Fig. 3. Extremum seeking scheme. The variable z denotes the Z-transform variable, h and γ are constants specifying the filters, ω denotes the frequency of the probing signal, a and b are the amplitudes of the sinusoidal signals.

Heat exchange takes place on all boundaries either by conduction or transportation. Note that “transportation” here refers to the internal energy being carried by the moving fluid mass. On the two walls the overall transportation is always zero. In fact, $\int_0^{L_z} \int_0^{L_x} (\mathbf{v}T)|_{y=0} dx dz - \int_0^{L_z} \int_0^{L_x} (\mathbf{v}T)|_{y=1} dx dz = (T_0 + T_d) \int_0^{L_z} \int_0^{L_x} [V(x, 0, z) - V(x, 1, z)] dx dz = 0$ in both uncontrolled and controlled cases. Hence, the heat fluxes at the bottom and the top are driven by conduction, which can be determined by the temperature gradient in the y direction:

$$I_b = -\frac{1}{\text{Pe}} \int_0^{L_z} \int_0^{L_x} \frac{\partial T}{\partial y} \Big|_{y=0} dx dz, \quad (3)$$

$$I_p = \frac{1}{\text{Pe}} \int_0^{L_z} \int_0^{L_x} \frac{\partial T}{\partial y} \Big|_{y=1} dx dz. \quad (4)$$

According to the Neumann boundary condition at the outlet, heat transfer is driven exclusively by transportation, i.e., the outlet heat flux is given by

$$I_e = \int_0^{L_z} \int_0^1 (\mathbf{v}T)|_{x=L} dy dz. \quad (5)$$

The Dirichlet boundary condition at the inlet allows conduction-driven heat transfer. However, for the case studies in this work the heat transfer is dominated by transportation, i.e., the inlet heat flux is written as

$$I_i = T_i \int_0^{L_z} \int_0^1 U|_{x=0} dy = QT_i. \quad (6)$$

The integrated heat flux balance $\int_{t_0}^{t_0+t_i} I_i + I_b + I_p - I_e dt$ should remain zero for long enough t_i . This serves as a basic consistency criterion for the heat transfer solver. Simulation results for stable flows agree very well with this equation, while turbulent flows may show slight disagreement.

III. EXTREMUM SEEKING FEEDBACK CONTROL

We propose a fixed-structure control law given by a traveling wave as the boundary condition, i.e.,

$$V_{ctrl} = V(y=0, 1) = A \sin[m(x - \theta t)], \quad (7)$$

where the constant A is the maximum amplitude, m is the wave number, and θ is the angular frequency, which is also called the phase speed in this work.

The performance of this fixed-structure control law is largely determined by m and θ , which control the spatial frequency and moving speed of the control “wave”. Note

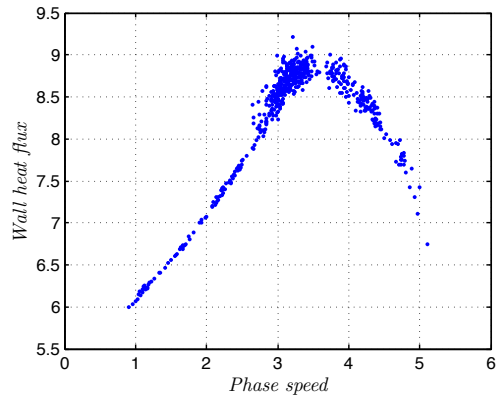


Fig. 4. Cost functions versus phase speed θ .

that m must take discrete integer values because the pseudo-spectral method used for the simulation study inherently requires the boundary conditions to be periodic in the x direction. Consequently, different values of m can be investigated separately in a parametric study. Indeed, simulation results show that a few choices can enhance flow turbulence and consequently the heat transfer rate. Based on the results of the parametric study, we adopt $m=2$ in this work. Regardless of the choice of m , the control “wave” needs to be in synchronization with the corresponding flow structures in order to enhance turbulence. In [13] we discussed a successful implementation of this strategy in a 2D channel flow, whose vortices are relatively constant and well-defined. In 3D channel flows, however, persistent flow structures are very rare. Nevertheless, the flow structures have a relatively steady moving speed, both in controlled and uncontrolled flows. Assuming that the average moving speed of the flow structures is V_e , we need to achieve $\theta = V_e$ in order to optimally actuate the flow structures. The choice of θ is more difficult than the choice of m because its value does not be an integer number. Moreover, many factors affects the moving speed of the flow structures, including the geometric settings, the physical properties of the fluid, the mass flux, the pressure gradient and the boundary control itself. The presence of significant measurement noise and undetermined system dynamics further complicates the problem. A clear understanding of the complex interaction among these factors is a highly challenging task. The goal of the feedback control design is to optimize the phase speed θ in real time in order to maximize a cost function related to heat transfer regardless of these factors.

It is natural then to seek a scheme that can automatically adjust the parameter θ in order to drive the system to an optimal or suboptimal state. One possible additional goal is to make such scheme robust against unmodeled system dynamics. With this goal in mind, in this work we follow a non-model-based approach to the problem where an accurate representation of the relationship between the boundary controls and the flow properties is not required. Extremum seeking, a non-model-based real-time optimization scheme, has been proved effective for a wide range of linear and nonlinear optimization problems where no reliable dynamic

system models are available. This makes extremum seeking an ideal candidate for optimally tuning in real time the value of θ in order to maximize a functional related to heat transfer.

The block diagram of the extremum seeking method is illustrated in Fig. 3. At each iteration step k , the flow is let evolve with a traveling wave of phase speed $\theta(k)$ as boundary condition. The phase speed $\theta(k)$ contains a superimposed sinusoidal perturbation (modulation). A given cost function J related to the heat transfer rate of the channel flow is evaluated using the response of the system to the phase speed $\theta(k)$. The cost function signal is then filtered by a high-pass filter and multiplied by another sinusoidal signal of identical frequency (demodulation). The demodulated signal ξ , containing gradient information of the system, is filtered through a low-pass filter and used to generate an updated phase speed $\theta(k+1)$ to be used during the next iteration step. A detailed explanation of this optimization scheme can be found in [14].

The to-be-maximized cost function is defined in this work as the overall wall heat flux $I_b + I_p$ defined in (3)-(4). Note that for a real application the integrals can just be approximated by sums of pointwise measurements. This cost function measures the overall heat flux from the walls to the fluid. Snapshots of the heat flux are taken every 40 simulation steps and the standard deviation of the collected data is calculated using the last 40 snapshots. Once this standard deviation decreases below a specific threshold, we consider the flow statistically steady and the cost function J is computed by averaging the heat flux rates over the same period of time used for the standard deviation calculation.

Extremum seeking is very effective in optimizing systems with cost functions that are smooth and with a well-defined extremum. However, extremum seeking may not capture the gradient information and fail if the cost function is not smooth or even discontinuous. Such situation does arise to some extent in our work, as the cost function shows sudden changes near the optimal point. The complexity of the cost function is shown in Fig. 4 as a function of the phase speed θ . The simulations are done with the following parameters: $Re = 400$ and $N = 0.1$. Although a clear trend can be noticed from the figure, the cost function seems sensitive to phase speed changes, especially near the optimal point ($\theta \approx 3.5$). Let us take, for instance, two data points in Fig. 4. The cost function drops from 9.21 to 8.77 when the phase speed changes from 3.2088 to 3.2093. This discontinuous behavior is largely caused by the nonlinearity of the flow. It may take extensive long time for the flow to reach the statistically steady state, and, because of this, the standard deviation criteria may simply fail to detect the convergence correctly. Furthermore, a flow with specific physical settings may have more than one statistically steady state and may not converge to the state with the highest cost function value. Since the sudden changes in the cost function value can cause unexpected disruptions during the optimization process, we have to make careful choices for the extremum seeking parameters in order to balance the efficiency and the stability of the extremum seeking algorithm.

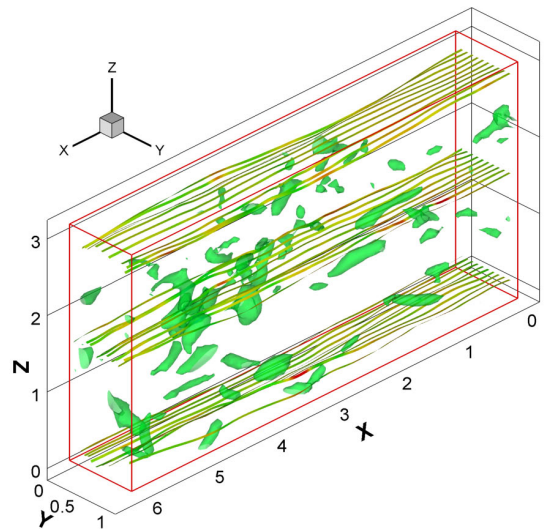


Fig. 5. Pressure isosurfaces ($p=0.8$) and streamline ribbons for an uncontrolled developed flow ($B_0=0$, $Re=400$). Color is coded by pressure.

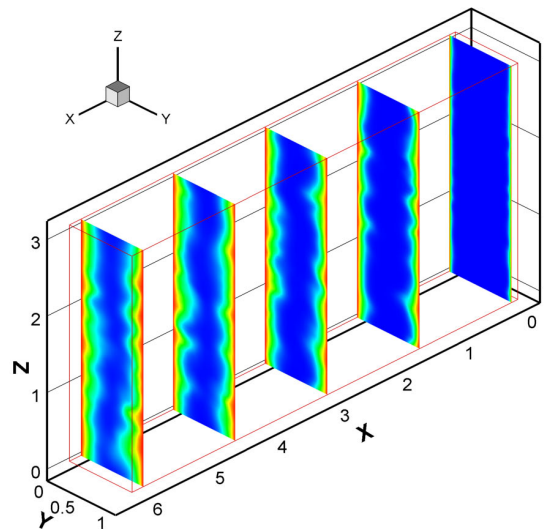


Fig. 6. Temperature maps of a fully developed flow ($Re=400$).

IV. SIMULATION RESULTS

The velocity-field numerical simulations are carried out by a modified Navier-Stokes solver, originally written by T. Bewley [21]. The equations are discretized using Fourier transforms on the streamwise direction and finite differences on the wall-normal direction, which is also called the pseudospectral method. Time integration is done using a fractional step method along with a hybrid Runge-Kutta/Crank-Nicolson scheme. Linear terms are treated implicitly by the Crank-Nicolson method and nonlinear terms are treated explicitly by the Runge-Kutta method. The divergence-free condition is fulfilled by the fractional step method [22].

A separate heat transfer solver is used to simulate the temperature-field evolution. Due to the limitations of the pseudospectral method for imposing boundary conditions at the channel inlet and outlet, a finite difference method is employed to solve the heat exchange problem. The grid is identical to the one used for the velocity-field pseudospectral

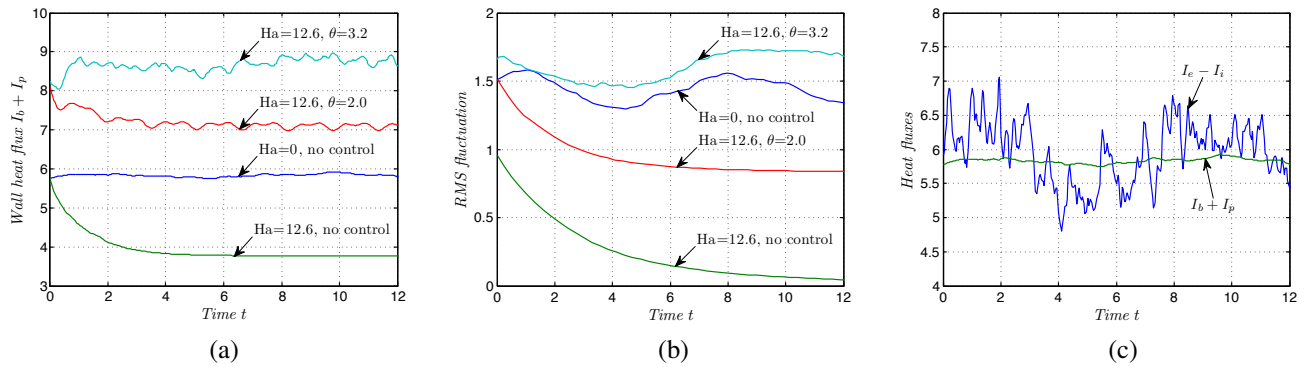


Fig. 7. (a) Wall heat flux, (b) RMS fluctuation, (c) Heat flux on the walls.

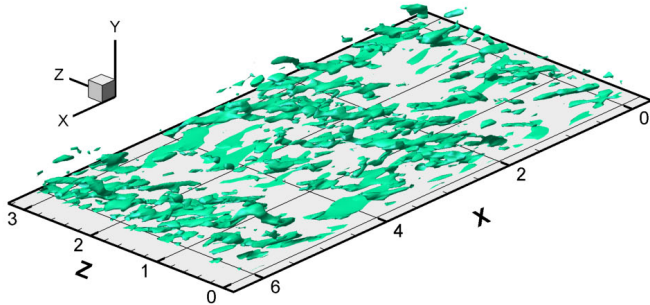


Fig. 8. Isosurfaces of ω_x

method. The temperature is defined at the same locations where the streamwise component of the velocity field is defined. The heat transfer equation is linear, given the fact that the velocity field is solved separately and known when the temperature field is solved. This enables implicit time integration of the heat transfer equation, which is carried out in this work using the Crank-Nicolson method. To ensure physical consistency for the heat transfer equation, an upwind scheme is necessary. Otherwise, meaningless spots hotter than $T_0 + T_d$ or colder than T_0 may appear. The Alternating Direction Implicit (ADI) method is used to avoid solving a large-scale sparse linear system. For more details on the implementation of these techniques, see [19].

All the simulations are carried out for the same flow domain: $0 < x < 2\pi$, $0 < y < 1$ and $0 < z < \pi$. The same mesh is used in all the simulations presented in this section (grid points in the x , y and z directions are identical: $N_x = N_y = N_z = 64$). The insensitivity of the results to resolution changes proves the adequacy of the grid. We consider $T_0 = 5$ and $T_d = 2$ in all cases. Similarly, we adopt $Q = 7.0$.

A. MHD flows with no control

When $B_0 = 0$, the momentum equation reduces to the standard incompressible Navier-Stokes equation characterizing the well-known Poiseuille flow. Poiseuille flows in 3D channels can be linearly stable for low Reynolds numbers, as infinitesimal perturbations in the flow field are damped out. The flows turn linearly unstable for high Reynolds numbers [23], [24]. Such flows usually reach statistically steady states, which we call fully established flows. By using pressure isosurfaces and streamline ribbons, Fig. 5 shows a typical fully established channel flow ($Re=400$).

The flow pattern inside the channel has a significant influence on heat exchange. The major portion of the flow structures is characterized by secondary circulations in the x - z plane. In fact, the temperature map in Fig. 6 suggests that the hot fluid near the walls is brought into the flow core by these circulations. As shown in Fig. 7(a), the vortices near the wall significantly increase the heat transfer rate I_b and I_p . The differences in the achieved heat transfer levels are closely related to the disturbance levels of the different flows, which can be further quantified by the RMS fluctuations in Fig. 7(b), defined as

$$\frac{1}{\pi} \frac{1}{2\pi} \left[\int_0^\pi \int_0^1 \int_0^{2\pi} |\mathbf{v}(x, y, z, t) - \bar{\mathbf{v}}(y, t)|^2 dx dy dz \right]^{\frac{1}{2}}, \quad (8)$$

where $\bar{\mathbf{v}}(y, t) = \frac{1}{\pi} \frac{1}{2\pi} \int_0^\pi \int_0^{2\pi} \mathbf{v}(x, y, z, t) dx dz$. The RMS fluctuation is commonly used to quantify the overall disturbance of the velocity field.

When $B_0 \neq 0$, the curve labeled with “Ha=12.6, no control” in Fig. 7(a) shows the effect of the imposed transverse magnetic field on the heat transfer capability of the channel for a positive Hartmann number, given by $Ha = B_0 L \sqrt{\sigma / \rho \nu} = \sqrt{N} Re$. As shown by the curve labeled with “Ha=12.6, no control” in Fig. 7(b), the RMS fluctuation is significantly lower than the pure hydrodynamic flow (indicated by the curve labeled “Ha=0, no control”) as the flow is stabilized by the imposed magnetic field. We can see that stronger imposed magnetic fields tend to make the flow more stable, resulting in a lower overall heat transfer rate.

Since the heat inflow $I_i = QT_i$ is constant, and the overall heat flux must be balanced, the heat outflow I_e must increase. By examining the wall heat flux and the outlet heat flux in Fig. 7(c), we can see that they provide similar information on the overall heat flux (Note that the curve labeled with “Ha=0, no control” in Fig. 7(a) is identical to the outlet heat flux in Fig. 7(c)). Physically, both quantities can be measured with proper equipment, which is readily available. For instance, the wall heat flux can be calculated by measuring temperature gradients in the y direction using temperature sensors embedded inside the wall. Outlet heat flux can be computed by measuring average temperature downstream. Note that the outlet heat flux contains a significant higher level of fluctuation. This is the primary reason to choose the wall heat flux over the outlet heat flux as the cost function.

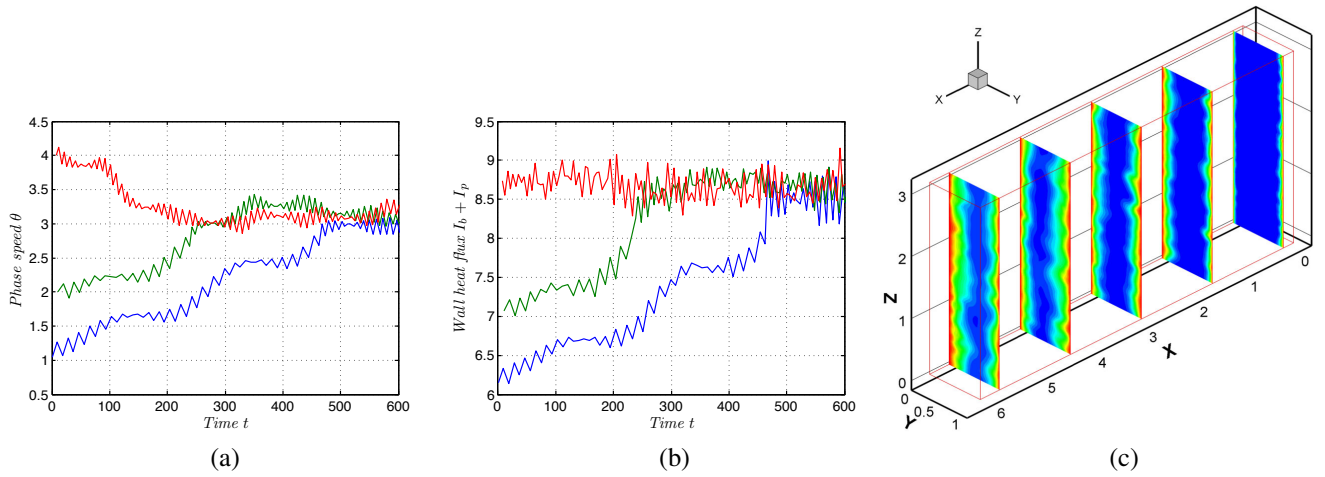


Fig. 9. Case 1 results: (a) Phase speed, (b) Cost function, (c) Temperature map at optimal state ($Re=400$).

B. MHD flows with extremum-seeking feedback control

Before illustrating the effectiveness of the extremum seeking scheme in optimizing the phase speed θ , we investigate the effect of different values of phase speed on the open-loop boundary control given by (7). Two values of θ , 2.0 and 3.2, at $Re=400$, $Pe=240$ and $Ha=12.6$ are studied. The open-loop control increases the wall heat flux to different levels, according to different the different values of phase speed. Note that the latter value, $\theta = 3.2$, is very close to the optimal phase speed as indicated by Fig. 4. As shown in Fig. 7(a) and Fig. 7(b), the $\theta = 3.2$ phase speed provides a significantly better result than the $\theta = 2.0$ phase speed in terms of both wall heat flux and RMS fluctuation. The flow pattern of the $\theta = 3.2$ case can be seen in Fig. 8, which shows the isosurfaces of the vorticity component in the x direction $\omega_x = \partial w / \partial y - \partial v / \partial z$ in the bottom half of the channel ($0 < y < 0.5$). Most of the flow structures stretch in the x direction, similar to Fig. 5. The $\theta = 2.0$ case has no such flow structures, indicating that the flow is still laminar despite the boundary control is applied. This proves that the phase speed has to be optimized before the boundary control can generate real turbulence.

Extremum seeking simulations are conducted for two cases. Case 1: $Re=400$, $Pe=240$, $Ha=12.6$. Case 2: $Re=400$, $Pe=240$, $Ha=6.3 \rightarrow 12.6$ at $t = 693$. The simulations start with the equilibrium solutions achieved after the external magnetic fields are imposed. The optimal extremum-seeking controller is expected to drive these flows to states with higher wall heat flux $I_b + I_p$. The parameters of the boundary controller are fixed as $A=0.12$ and $k=1$. The extremum seeking parameters have to be carefully chosen to balance stability and performance of the optimization process. In our cases, we use: $a=0.12$, $\gamma=0.12$, $\omega=3$, $h=0.8$, $b=1$.

In Case 1, we investigate several choices of initial phase speed: 1.0, 2.0 and 4.0. As we can see from Fig. 9(a) and Fig. 9(b), the extremum seeking algorithm successfully drives the boundary control to a value that maximizes the wall heat flux. We can note from Fig. 9(a) that even though the controller cannot keep the system at the optimal phase

speed all the time, it manages to stabilize the phase speed near the optimum, regardless of significant amount of randomness in the cost function.

An imposed magnetic field with moderate strength can completely laminarize the flow and reduce the heat exchange to a very low level. From Fig. 7(a) we can see that the wall heat flux in a highly stabilized flow is around 3.8 (curve labeled with “ $Ha=12.6$, no control”), while the wall heat flux in a fully developed flow when no magnetic field is present is around 5.9 (curve labeled with “ $Ha=0$, no control”). This implies that the elimination of the the vortices due to the imposition of a magnetic field produces a 36% decrease in the heat exchange rate. Fig. 9(b) shows that the extremum seeking controller succeeds in increasing the wall heat flux to 8.8 (curve labeled with “ $Ha=12.6$, $\theta = 3.2$ ”), which is 51% higher than the level achieved by the fully developed flow when no magnetic field is present, and 134% times higher than level achieved by the completely laminarized flow due to the presence of the magnetic field. Note that even though a non-optimal boundary actuation (curve labeled with “ $Ha=12.6$, $\theta = 2.0$ ”) cannot overcome the laminarization of the flow and its associated overall RMS fluctuation level is below the level associated with the fully developed flow when no magnetic field is present, it still can increase the wall heat flux since most of the unsteadiness is introduced near the walls. The effect of the enhanced unsteadiness on the wall heat flux can be clearly seen in the temperature maps shown in Fig. 9(c). A comparison with Fig. 6 indicates that in a controlled flow the cool fluid from the inlet can mix with the hot fluid near the walls more efficiently, thus increasing the heat transfer between the fluid and the walls.

Case 2 emphasizes the capability of the extremum-seeking-based controller to easily adapt to changing flow conditions without the need of changing its parameters. This case assumes a weaker initial external magnetic field than the one applied to the flow in Case 1, resulting in a smaller Ha number. The simulation starts with an initial phase speed of 5.0. The evolution of the phase speed and the wall heat flux are shown in Fig. 10(a) and Fig. 10(b). We can see that after a short transient period the phase speed converges to an

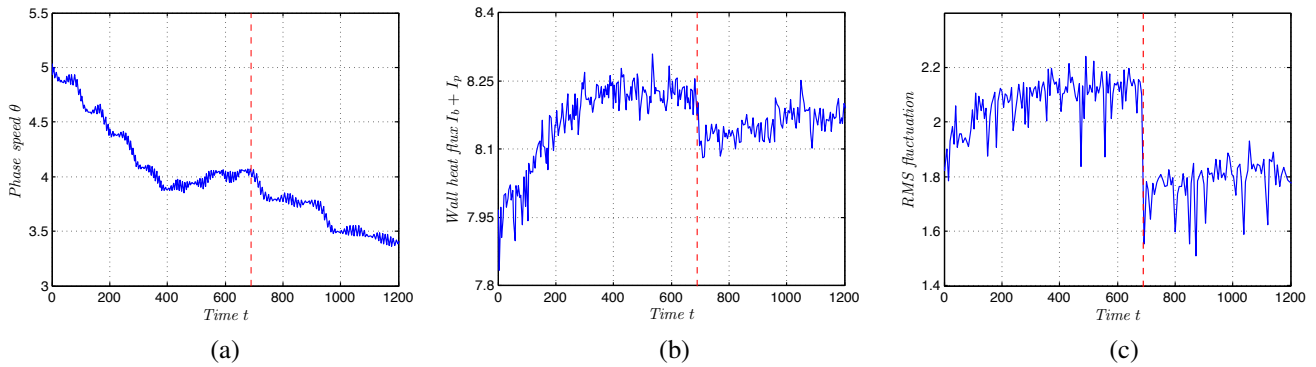


Fig. 10. Case 2 results: (a) Phase speed, (b) Cost function, (c) RMS fluctuation.

optimal value of around 4.0, whose corresponding wall heat flux is slightly better than that in Case 1. This is expected because the flow with lower Hartmann number is inherently less stable. Then, at $t=690$ (the instance is identified by a red dashed line) the external magnetic field strength is doubled (same level as used in Case 1). This sudden alteration of the physical setting results in a moderate change of the flow dynamics and the optimal value of the phase speed. As shown in Fig. 10(a) and Fig. 10(b), the extremum seeking controller quickly adjusts the phase speed as a response to the change in the system output value and seeks a new optimal value that maximizes the wall heat transfer. In Fig. 10(c), the RMS fluctuation also shows a dramatic change after the external magnetic field is suddenly increased, which is consistent with the change in the heat flux.

V. CONCLUSION

A boundary feedback control scheme based on a fixed-structure controller optimally tuned by extremum seeking has been proposed for heat exchange enhancement in a 3D SMHD channel flow. Simulation results show that the control scheme can successfully destabilize the highly stable flow, increasing the heat exchange rate between the fluid and the channel walls. As a consequence, the fluid temperature at the channel outlet is significantly increased, maximizing in this way heat extraction. Because of the complexity of the MHD channel flow, significant discontinuities exist in the relationship between the to-be-maximized cost function and the to-be-optimized parameters. The tuning of the extremum seeking algorithm is crucial for the success of the scheme.

As part of our future research work, extremum-seeking-based control schemes will be developed using different actuation mechanisms. More robust methods to deal with the discontinuity of the cost function will be sought, especially when multiple parameters are optimized. Since a cost function with less or none discontinuity behavior is desirable, the choice of the cost function may also be reviewed.

REFERENCES

- [1] U. Müller and L. Bühler, *Magneto-fluid dynamics in Channels and Containers*. Springer, 2001.
- [2] M. D. Gunzburger, *Flow Control*, ser. The IMA Volumes in Mathematics and its Applications. New York: Springer-Verlag, 1995, vol. 68.
- [3] S. S. Srinitharan, Ed., *Optimal control of viscous flow*. SIAM, Philadelphia, 1998.
- [4] O. M. Aamo and M. Krstić, *Flow Control by Feedback*. Springer, 2002.
- [5] M. R. Jovanovic, "Turbulence suppression in channel flows by small amplitude transverse wall oscillations," *Physics of Fluids*, vol. 20, no. 1, p. 014101, 2008.
- [6] A. B. Tsinober, *Viscous Drag Reduction in Boundary Layers*, ser. Progress in Astronautics and Aeronautics. Washington, DC: AIAA, 1990, no. 123, ch. MHD Flow Drag Reduction, pp. 327–349.
- [7] H. Choi, D. Lee, and J. Lim, "Control of near-wall streamwise vortices using an electromagnetic force in a conducting fluid," *AIAA Paper*, vol. 97-2059, 1997.
- [8] T. Berger, J. Kim, C. Lee, and J. Lim, "Turbulent boundary layer control utilizing the Lorentz force," *Physics of Fluids*, vol. 12, p. 631, 2000.
- [9] K. S. Breuer, J. Park, and C. Henoeh, "Actuation and control of a turbulent channel flow using Lorentz forces," *Physics of Fluids*, vol. 16, no. 4, pp. 897–907, 2004.
- [10] E. Spong, J. Reizes, and E. Leonardi, "Efficiency improvements of electromagnetic flow control," *Heat and Fluid Flow*, vol. 26, pp. 635–655, 2005.
- [11] E. Schuster, L. Luo, and M. Krstić, "MHD channel flow control in 2D: Mixing enhancement by boundary feedback," *Automatica*, vol. 44, no. 10, pp. 2498 – 2507, 2008.
- [12] L. Luo and E. Schuster, "Heat transfer enhancement in 2D magnetohydrodynamic channel flow by boundary feedback control," *Proceedings of 45th IEEE Conference on Decision and Control*, pp. 5317–5322, San Diego, 2006.
- [13] —, "Boundary feedback control for heat exchange enhancement in 2D magnetohydrodynamic channel flow by extremum seeking," in *48th IEEE Conference on Decision and Control*, San Diego, Shanghai, China, pp. 5317–5322.
- [14] K. Ariyur and M. Krstić, *Real-time Optimization by Extremum-seeking Control*. Wiley-Interscience, 2003.
- [15] R. King, R. Becker, G. Feuerbach, L. Henning, R. Petz, W. Nitsche, O. Lemke, and W. Neise, "Adaptive flow control using slope seeking," *Proceedings of 14th Mediterranean Conference on Control and Automation*, pp. 1–6, June 2006.
- [16] J. Beaudoin, O. Cadot, J. Aider, and J. Wesfreid, "Bluff-body drag reduction by extremum-seeking control," *Journal of Fluids and Structures*, vol. 22, no. 6-7, pp. 973–978, 2006.
- [17] M. Pastoor, L. Henning, B. Noack, R. King, and G. Tadmor, "Feedback shear layer control for bluff body drag reduction," *Journal of Fluid Mechanics*, vol. 608, pp. 161–196, 2008.
- [18] G. Branover, *Magneto-hydrodynamic Flow in Ducts*. Halsted Press, 1979.
- [19] J. Anderson, *Computational Fluid Dynamics, the Basics with Applications*. McGraw-Hill, 1995, pp. 153–165.
- [20] H. Choi and P. Moin, "Effects of the computational time step on numerical solutions of turbulent flow," *Journal of Computational Physics*, vol. 113, no. 1, pp. 1–4, 1994.
- [21] T. R. Bewley, *Optimal and robust control and estimation of transition, convection, and turbulence*. Stanford University thesis, 1999.
- [22] J. Dukowicz and A. Dvinsky, "Approximate factorization as a high order splitting for the implicit incompressible flow equations," *Journal of Computational Physics*, vol. 102, no. 2, pp. 336–347, 1992.
- [23] R. L. Panton, *Incompressible flow*, 2nd ed. New York: Wiley, 1996.
- [24] P. J. Schmid and D. S. Henningson, *Stability and transition in shear flows*. New York: Springer, 2001, vol. 142.